ELSEVIER

Journal of Molecular Catalysis A: Chemical 192 (2003) 239–251

JOURNAL OF MOLECULAR CATALYSIS A: CHEMICAL

www.elsevier.com/locate/molcata

Pd/SiO_2 catalysts: synthesis of Pd nanoparticles with the controlled size in mesoporous silicas

Igor Yuranov [a], Pedro Moeckli [b], Elena Suvorova [c], Philippe Buffat [c], Lioubov Kiwi-Minsker [a,*], Albert Renken [a]

[a] *LGRC, Swiss Federal Institute of Technology, CH-1015 Lausanne, Switzerland*
[b] *DMX/LC, Swiss Federal Institute of Technology, CH-1015 Lausanne, Switzerland*
[c] *CIME, Swiss Federal Institute of Technology, CH-1015 Lausanne, Switzerland*

Received 23 April 2002; accepted 17 July 2002

Abstract

Synthesis of Pd nanoparticles with controlled size (d_{Pd} = 1–3.6 nm) was carried out within the pores of the mesoporous HMS and SBA-15 silicas. Pd was ion-exchanged on non-calcined silicas, prepared by solvent extraction of the templates. A high concentration of silanol groups on the mesopore surface allowed attaining Pd loading up to 4.4. wt.%. The Pd/HMS and Pd/SBA-15 were characterised by chemical analysis, XRD, N2 adsorption–desorption and transmission electron microscopy (TEM) methods. The materials possess a high SSA and narrow pore size distribution. Introduction of Pd nanoparticles in HMS resulted in a progressive loss of the regularity in the mesoporous structure. On the contrary, all Pd/SBA-15 composites retained the original well-ordered 2D hexagonal structure of SBA-15. The thick walls of the SBA-15 framework are accounted for the higher stability observed. The TEM investigations confirmed that the Pd nanocrystals were located within the SBA-15 mesoporous framework channels. The particle size did not exceed the mesopore diameter (2–6 nm) at Pd loading of 0.1–4.4 wt.%. Pd clusters were found to be resistant against sintering during air-calcination (550 °C, 4 h). The catalyst 2.1%Pd/SBA-15 used in methane combustion at 520 °C demonstrated stable activity during 6 h on stream.

Keywords: Mesoporous silica; HMS; SBA-15; Pd nanoparticles; Size-controlled synthesis

1. Introduction

Metal particles of nanometer size have unique characteristics that differ from those of individual atoms and bulk substances [1]. Thus, they acquire different heat capacity, vapour pressure [2], melting point [3,4], optical, magnetic and electronic properties. The latter together with a high surface-to-volume ratio and the increased number of edges, corners and faces lead to a higher activity and selectivity during catalytic reactions [5,6]. The understanding of the size effect in catalysis would allow tuning the catalytic activity and selectivity by changing the metal cluster size. However, the preparation of supported nanoparticles with a desired size still remains a challenge. Two major problems have to be solved: the first one is how to control the supported metal nanoparticle size, the second—how to maintain this size during the catalytic reactions, since under reaction conditions at elevated temperatures metal sintering usually takes place. Porous

* Corresponding author. Tel.: +41-21-693-31-82; fax: +41-21-693-31-90.
E-mail address: lioubov.kiwi-minsker@epfl.ch (L. Kiwi-Minsker).

1381-1169/02/$ – see front matter
PII: S1381-1169(02)00441-7

structures like zeolites provide a mechanism for confining metal clusters in controlled fashion [7–9]. In this case the particle size is determined by the size of the zeolite cells. When introduced into the zeolite channels, metal clusters have enhanced resistance to agglomeration, since they are isolated from each other in the solid matrix. However, in the case of very small zeolites pores (<2.0 nm) the diffusion of bulky organic substrates to the internal catalytically active sites is restricted.

Recently developed mesoporous silicates, such as M41S family [10–12], SBA-*x* [13–15], HMS [16], MSU-*x* [17], due to their unique properties have shown to be suitable supports for metal and metal oxide nanoparticles. These mesoporous molecular sieves possess high specific surface area (SSA) (700–1500 m^2/g), large specific pore volume (0.8–1.2 cm^3/g) and highly ordered pore structure with narrow size distribution. The pore size of these materials may be varied from 2 to 50 nm using different synthetic pathways [18]. As in the case of zeolites, the mesoporous framework may control the metal particle size limiting the growth of the clusters introduced into the confined space of the channels. Such nanostructured materials should have enhanced resistance to sintering, since the metal nanoparticles are isolated one from another by silica walls.

Besides pharmaceutical and fine chemistry, where the metal nanoparticles supported on mesoporous matrices may catalyse many important guest–host reactions, there are potential applications of these materials in different areas of nanotechnology, optics, electronics, adsorption, and separation [19]. Work has been directed toward the synthesis of nanoparticles (nanowires) of the metals, such as palladium [20–33], platinum [8,20,34–40], ruthenium [41–47], gold [48–51], silver [36,52], within the channels of mesoporous silicates, mainly, MCM-41. The metals were introduced into the support either directly during the mesoporous silicate synthesis, or by post-synthesis treatment. Direct incorporation was performed adding the metal precursor into the synthesis silica gel before ageing [34,37,45] or by a stabilisation of the metal precursor inside the template micelles during the self-assembly of the surfactant and silicate [30,32,47]. The post-synthesis metal deposition was carried out using a calcined mesoporous support via incipient wetness impregnation [35,39], ion-exchange [25–27,53], equilibrium adsorption, metal complex immobilisation [8,22], and vapour-phase grafting [23,31]. The extensively employed methods of support impregnation and addition of a metal precursor into the synthesis gel lead to the uncontrolled growth of metal particles inside the pores and on the external support surface, resulting in a broad particle size distribution. The vapour-phase deposition, metal complex immobilisation and introduction of a metal precursor inside the template micelles seem to allow the control of metal particle growth within the pores. However, these methods are rather difficult to handle and require stringent reaction conditions, like vacuum, non-aqueous solvents, organometallic precursors, etc. The ion-exchange of silanol groups with precursor cations is the common technique used for the metal deposition on the internal wall surface of the mesopores. However, in this case a relatively low ion-exchange capacity of the calcined support limits the metal loading, for example, by ∼1 wt.% for Pd [25–27,53]. Only few syntheses of size-controlled noble metal nanoparticles within the channels of mesoporous molecular sieves have been described [8,25,28,29,33]. No systematic investigation of the influence of the synthesis conditions (mesoporous support pre-treatment, metal loading, etc.) on the properties of metal/mesoporous silica composites has been reported.

The present work was aimed on the synthesis of Pd nanoparticles within the framework channels of HMS and SBA-15 mesoporous molecular sieves addressing: (i) the size control of Pd particles confined within the mesopores, (ii) the incorporation of Pd at high loading and (iii) the resistance of the Pd/mesoporous silica structure against a collapse and sintering at elevated temperatures. Ion-exchange of silanol groups with $[Pd(NH_3)_4]^{2+}$ cations was chosen as a method of metal deposition. In order to obtain a high concentration of silanol groups on the mesopore surface, before ion-exchange the templates were removed by a solvent extraction [54].

2. Experimental

The chemicals (purum, Fluka, Aldrich): tetraamminepalladium(II) chloride monohydrate ($Pd(NH_3)_4Cl_2 \cdot H_2O$), tetraethoxysilane (TEOS), dodecylamine

(DDA), octadecylamine (ODA), poly(ethylene glycol)–poly(propylene glycol)–poly(ethylene glycol) triblock copolymer, $EO_{20}PO_{70}EO_{20}$ (Pluronic 123, $M_{av} = 5800$), ethanol (EtOH), methanol (MeOH), were used as received. Deionised water was employed during the synthesis.

2.1. Synthesis of mesoporous silicas

Hexagonal molecular sieves (HMS) were prepared via a neutral (S^0I^0) templating route as described elsewhere [55]. The primary amines—dodecylamine and octadecylamine—were used as neutral structure directors in order to control a pore size of the resulting mesoporous silicas [16]. In a typical preparation, DDA (4.15 g) was dissolved in 55 ml of ethanol, and then 75 ml of H_2O were added to the solution. The synthesis was carried out at 55 °C. TEOS (20 ml) was added to the surfactant solution resulting in a reaction mixture with a ratio TEOS:DDA:EtOH:H_2O of 4:1:41.5:170. The mixture was vigorously stirred in sealed flask at 55 °C for 20 h. The resulting white precipitate was filtered, washed by water and dried at room temperature. Template removal was achieved either by calcination at 550 °C for 4 h (heating rate: 2 °C/min) or by solvent extraction. The solvent extraction was performed by stirring 1 g of the product in 150 ml of ethanol (45 °C) for 1 h. The extraction was repeated three times with pure ethanol. The final product was air-dried over night. The same procedure was applied for the synthesis with ODA.

Hexagonally ordered SBA-15 was synthesised in acidic media via an (S^0H^+) (X^-I^+) synthetic route using poly(ethylene glycol)–poly(propylene glycol)–poly(ethylene glycol) triblock copolymer, $EO_{20}PO_{70}EO_{20}$ (Pluronic 123) as a templating agent [15]. In a typical preparation, 8 g of Pluronic 123 was dissolved in 60 ml of water and 240 ml of 2N HCl solution at 35 °C. After addition of 18.2 ml of TEOS the reaction mixture was stirred first at 35 °C for 24 h and then at 80 °C for 48 h. The final solid product was recovered by filtration, washed with water and air-dried at room temperature. Template removal was performed by calcination and by solvent extraction as described above for the HMS materials.

All prepared mesoporous silicas are listed in Table 1. The suffixes "-calc." and "-extr." identify the calcined supports and the supports treated by solvent extraction, respectively. The number of aliphatic carbon atoms in the primary amines used as templates is specified in brackets.

2.2. Formation of Pd nanoparticles in the mesoporous silicas

Palladium was introduced into the synthesised mesoporous silicas via ion-exchange from $Pd(NH_3)_4Cl_2$ aqueous solution. The mesoporous silicas prepared by solvent extraction of the template were commonly used for the Pd clusters formation. To study the influence of the support pre-treatment on the Pd particles dispersion, calcined HMS(12) was also used. Pd loading was varied from 0.1 to 4.4 wt.%.

In a typical synthesis, the amount of $Pd(NH_3)_4Cl_2$ corresponding to a selected Pd loading was dissolved in 40 ml of H_2O. One drop of aqueous NH_3 (10 wt.%) was added reaching pH ∼8. The high pH of ion-exchange solution was reported to destroy the mesoporous structure [38]. Mesoporous silica (1 g) was introduced in the prepared ion-exchange solution, and the mixture was stirred vigorously at room temperature for 4 h. The resulting solid was filtered out, washed carefully (three times, stirring for 0.5 h) with water and air-dried over night. Afterwards, all products were slowly heated up to 550 °C (temperature ramp: 2 °C/min) in air and calcined at 550 °C for 4 h. Before the transmission electron microscopy (TEM) investigations, the calcined samples were reduced by H_2 at 300 °C for 1 h. In some cases, the as-synthesised materials were reduced by H_2 at 300 °C for 1 h without calcination.

The physicochemical properties of the synthesised Pd-mesoporous silica composites are listed in Table 1.

2.3. Characterisation of materials

Chemical analysis of the samples was carried out using atomic absorption spectroscopy (AAS) via Shimadzu AA-6650 with air-acetylene flame. For the analysis the samples were dissolved in hot aqua regia containing several drops of HF.

The specific surface area of the supports and the catalysts were measured using N_2 adsorption–desorption at −196 °C by a Sorptomatic 1990 (Carlo Erba) instrument. Before the measurements catalysts were heated in vacuum at 250 °C for 2 h. The SSA of the samples

Table 1
The main characteristics of the mesoporous silicas and Pd/SiO_2 composites

Sample	Template	N_2 adsorption–desorption measurements			Pd loading (wt.%)	Average Pd particle diameter (nm)[a]	Pd dispersion (%)[a]	d_{100} (nm)	$a_0 = d_{100} \times 2/\sqrt{3}$ (nm)	Wall thickness, $b = a_0 - D$ (nm)
		SSA (m^2/g)	Pore volume, V_t (cm^3/g)	Pore size, D (nm)						
HMS(12)-calc.	DDA	1015	1.65	2.6	–	–	–	4.3	5.0	2.4
HMS(12)-extr.		870	1.39	2.6	–	–	–	4.4	5.1	2.5
0.2%Pd/HMS(12)-extr.		1012	1.65	2.5	0.2	0.9	~100	–	–	–
0.9%Pd/HMS(12)-extr.		1010	1.67	2.5	0.9	1.7	68	–	–	–
2.1%Pd/HMS(12)-extr.		990	1.71	2.4	2.1	1.9	57	–	–	–
0.2%Pd/HMS(12)-calc.	DDA	1035	1.79	2.5	0.2	8.0	14			
0.5%Pd/HMS(12)-calc.		1030	1.75	2.5	0.5	8.8	13	4.5	5.2	2.7
HMS(18)-calc.	ODA	885	1.21	3.3	–	–	–	5.1	5.9	2.6
0.1%Pd/HMS(18)-extr.		820	1.21	3.3	0.1	1.2	96	–	–	–
0.25%Pd/HMS(18)-extr.		645	1.33	3.5	0.25	1.9	57	–	–	–
1.0%Pd/HMS(18)-extr.		690	0.99	3.5	1.0	1.8	64	–	–	–
1.4%Pd/HMS(18)-extr.		690	1.11	3.6	1.4	1.4	82	–	–	–
4.4%Pd/HMS(18)-extr.		655	0.86	3.6	4.4	1.7	68	–	–	–
SBA-15-calc.	Pluronic 123	875	1.22	6.1	–	–	–	9.2	10.6	4.5
SBA-15-extr.		801	0.98	5.2	–	–	–	9.6	11.1	5.9
0.6%Pd/SBA-15-extr.		808	0.96	5.1	0.6	3.6	32	9.4	10.8	5.7
2.1%Pd/SBA-15-extr.		730	0.99	5.1	2.1	3.5	34	9.1	10.5	5.4
2.1%Pd/SBA-15-red.[b]		820	0.98	5.1	2.1	1.0	~100			

Extr.: extraction; calc.: calcined; red.: reduced.

[a] Pd dispersion and average particle diameter were measured by CO pulse adsorption.

[b] The as-prepared 2.1%Pd/SBA-15-extr. was reduced by H_2 (300 °C) without calcination.

was calculated employing the BET method while the Dollimore/Heal method was applied for the calculation of pore volume and pore size distribution (PSD).

The SSA of Pd and its dispersion were measured by CO pulse adsorption (3 vol.% CO in He) at 50 °C via a Micromeritics 2910. The samples were pre-treated in a flow of H_2 at 300 °C during 1 h and subsequently in He flow at 300 °C during 1 h. The HRTEM investigation showed that palladium supported on the mesoporous silicas was fully reduced under these conditions to metallic state. A Pd surface density of 1.2×10^{19} atoms/m^2 and a stoichiometry factor SF_{Pd} = CO/Pd of 0.6 were used for the SSA_{Pd} calculations.

X-ray diffraction (XRD) spectra were performed on a D500 Siemens powder diffractometer (Cu Kα_1) in the angle range of 0.5–10° 2Θ with the steps of 0.02° and a step time of 8 s.

Transmission electron microscopy was applied to characterise Pd nanoparticles confined in mesoporous silica. The TEM samples were prepared by gently settling the powder on a holey carbon film supported by a copper grid. Grains with suitable orientation and small enough to be transparent for the electron beam were chosen for observation the mesoporous structure and Pd particle dispersion. In order to reduce the thickness of the silica matrix and to increase the Pd particles contrast, some samples were prepared by ultramicrotomy. For this purpose the powder sample was embedded in epoxy and cut with a 45° diamond knife at room temperature. Slices of 20–50 nm thickness were picked up from the water surface by means of a metallic loop and transferred on the holey carbon film for the examination.

Morphology characterisation of both the support and Pd nanoparticles were carried out by TEM in a Philips CM300UT FEG with 300 kV field emission gun, 0.65 mm spherical aberration and 0.17 nm resolution at Scherzer defocus. The images were recorded on a Gatan 797 slow-scan CCD camera (1024 × 1024 pixels) and processed with the Gatan Digital Micrograph 3.4.4 software for contrast enhancement. TEM bright field contrast was mostly used although the Pd particles contrast was low in the mesoporous matrix. High-resolution (HRTEM) images of the palladium lattice established the crystalline nature of the particles. The scanning TEM mode was used to provide higher atomic number Z-contrast for the overview observation of Pd nanoparticles. However, its resolution (∼0.3 nm) resulted in some loss of information for the smallest Pd clusters.

2.4. Measurement of catalytic activity in total oxidation of methane

For the catalytic activity measurements the calcined 2.1%Pd/SBA-15-extr. sample was pelletised, crushed in a mortar and sieved. The fraction with a particle size of 0.3–0.5 mm was used. The methane oxidation was carried out in a continuous flow fixed-bed reactor [56] operated as a plug flow reactor. The catalyst (∼0.1 g) was placed into the middle section of the reactor. To avoid as much as possible a gas flow maldistribution, quartz beads were placed before and after the catalyst in the catalytic bed. A gas mixture of 1 vol.% methane and 10 vol.% oxygen in argon was used for the catalytic tests. The methane, oxygen and argon (provided by Carbagas, Lausanne, Switzerland, >99.99%) were used as received without any purification. The gas flow was controlled by mass flow controllers. The total gas flow of 100 ml/min (STP) was used throughout the study. The reaction temperature was monitored by a thermocouple placed in the catalytic bed. The outlet carbon monoxide and carbon dioxide concentrations were continuously monitored by an infrared analyser Ultramat 22P (Siemens).

3. Results and discussion

The nitrogen adsorption–desorption isotherms and XRD patterns of the template-derived silicas are presented in Figs. 1–5. These isotherms are typical for well-defined mesoporous frameworks [14,16]. All materials show a high specific surface area, specific pore volume and narrow pore size distribution (Table 1).

The HMS molecular sieves, prepared with the alkylamines as structure-directing agents, exhibit a single low angle reflection in the X-ray diffraction patterns. Higher order reflections were not resolved. Nevertheless, it is assumed that these materials possessing a wormhole framework structure can exhibit local hexagonal symmetry [55,57]. As the surfactant chain length increased from C_{12} to C_{18}, the position of the single (1 0 0) reflection shifts toward lower 2Θ

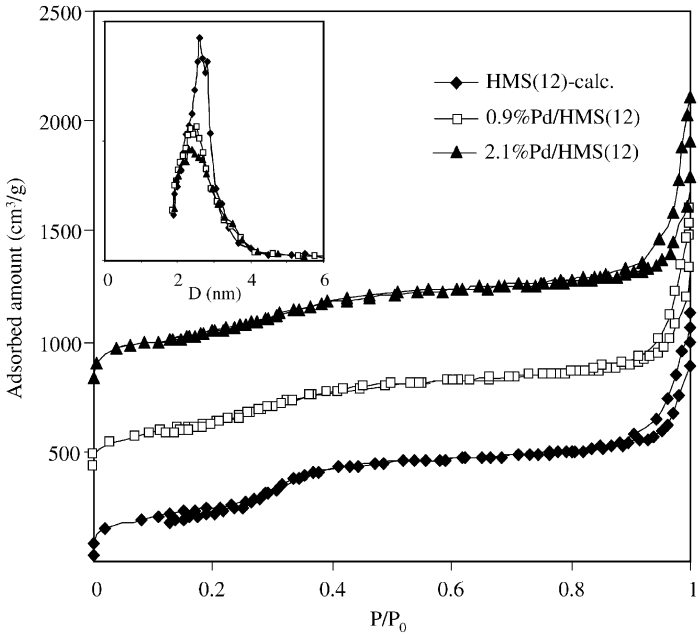

Fig. 1. N_2 adsorption–desorption isotherms of the HMS(12)-calc. and Pd/HMS(12)-extr. materials. For a better comparison, data for the 0.9%Pd/HMS(12)-extr. and 2.1%Pd/HMS(12)-extr. were shifted by 400 and 800 units, respectively. Inset: pore size distribution.

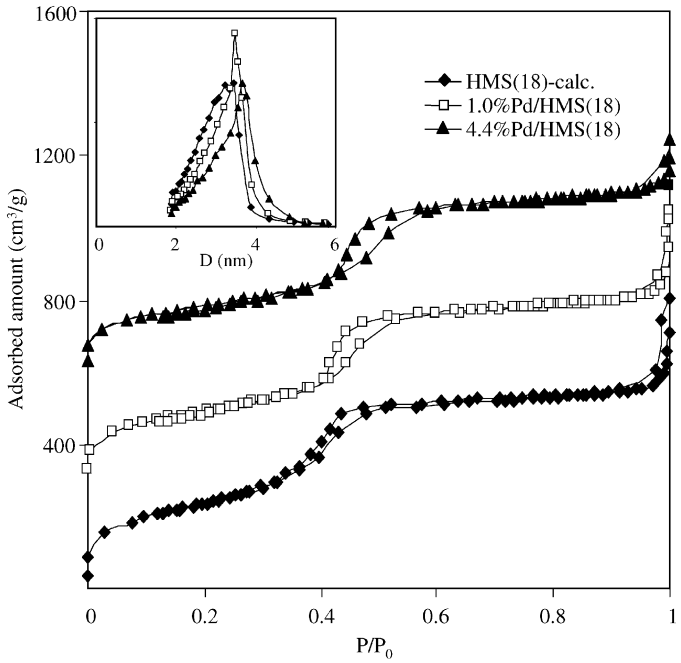

Fig. 2. N_2 adsorption–desorption isotherms of the HMS(18)-calc. and Pd/HMS(18)-extr. materials. For a better comparison, data for the 1.0%Pd/HMS(18)-extr. and 4.4%Pd/HMS(18)-extr. were shifted by 300 and 600 units, respectively. Inset: pore size distribution.

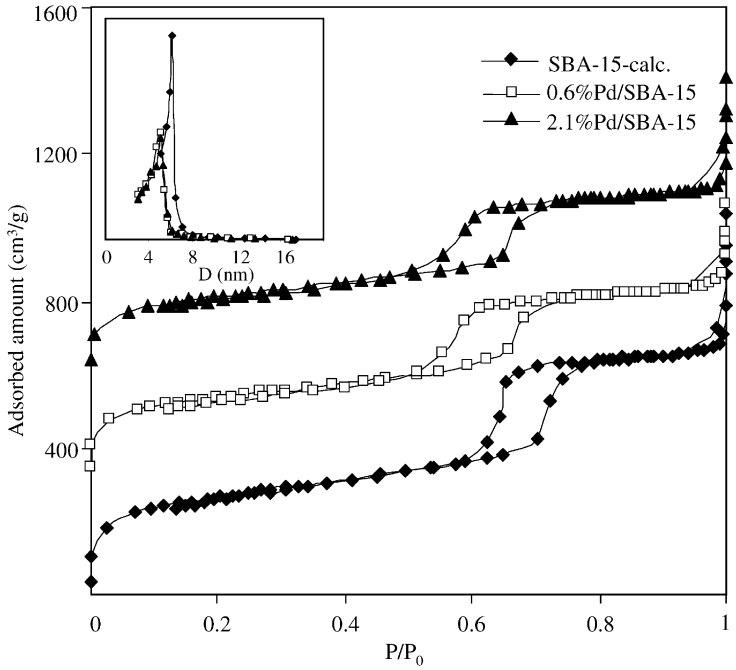

Fig. 3. N_2 adsorption–desorption isotherms of the SBA-15-calc. and Pd/SBA-15-extr. materials. For a better comparison, data for the 0.6%Pd/SBA-15-extr and 2.1%Pd/SBA-15-extr. were shifted by 300 and 600 units, respectively. Inset: pore size distribution.

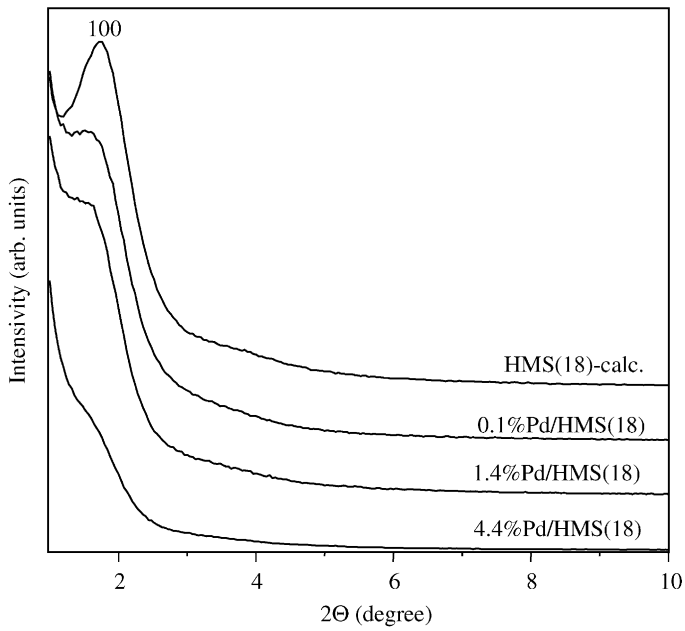

Fig. 4. XRD patterns of the HMS(18)-calc. and Pd/HMS(18)-extr. materials.

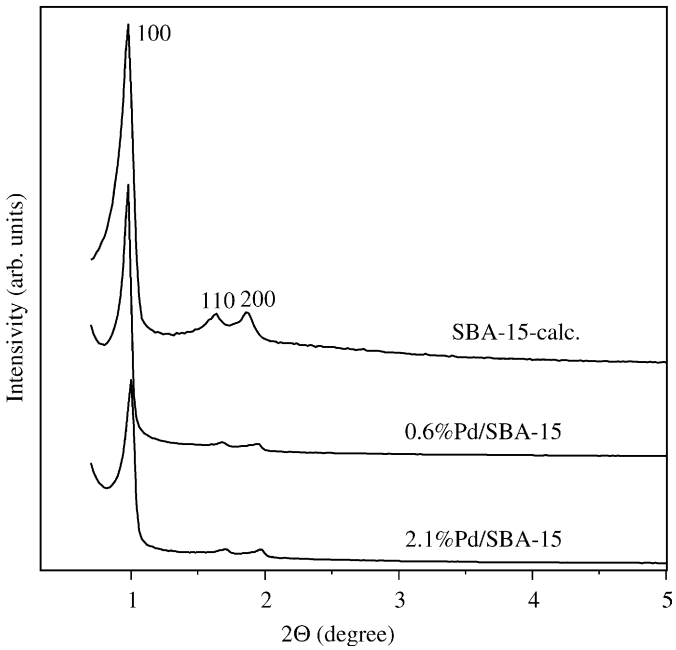

Fig. 5. XRD patterns of the SBA-15-calc. and Pd/SBA-15-extr. materials.

values, indicating the increase of the average distance between the pore centres. At the same time the N_2 adsorption–desorption measurements show that the mesopore diameter, which corresponds to the diameter of the template rodlike micelles, increases from 2.6 to 3.3 nm for the calcined samples. Thus, the diameter of the HMS framework channels can be varied by applying the surfactants with different alkyl chain lengths [16,57].

The SBA-15-calc., prepared using $EO_{20}PO_{70}EO_{20}$ (Pluronic 123) as a templating agent, demonstrates three well-resolved diffraction peaks with $d = 9.2$, 5.4, and 4.6 nm, which can be indexed as the (1 0 0), (1 1 0) and (2 0 0) reflections associated with *p*6*mm* hexagonal symmetry [14]. The SBA-15-calc. was found to have the mesopore size of 6.1 nm (Table 1). The framework wall thickness, which can be estimated by subtracting the pore diameter from the repeat distance a_0 between pore centres of hexagonal structure (calculated from XRD data using the formula $a_0 = 2d_{100}/\sqrt{3}$ [15]), is almost the same for HMS(12)-calc. and HMS(18)-calc. (2.4–2.6 nm). The wall thickness calculated for the SBA-15-calc. is significantly bigger (4.5 nm). The N_2 adsorption and XRD measurements confirm that after material synthesis the surfactants can be effectively removed by solvent extraction as well as by calcination. After template extraction the materials retain all parameters of the mesoporous structures (Table 1).

Though both calcined and non-calcined mesoporous silica samples were used for palladium deposition via ion-exchange, more emphasis was made on the non-calcined supports prepared by solvent extraction of the templates. The main advantage of the extracted materials compared to the calcined ones, is the higher amount of silanol groups [54] providing higher pore surface functionality. In order to study the influence of the support pre-treatment on the resulting metal particle size, ion-exchange with Pd^{2+}-ions, was carried out for the HMS(12)-extr. and HMS(12)-calc. samples. In the latter case an average Pd particle size was found to be 8–9 nm exceeding the average pore diameter (Table 1). In the case of the extracted HMS(12) support, the palladium particle sizes were always within the range of the mesopore diameters (2.4–2.6 nm). Thus, the low concentration of silanol groups on the inner pore surface of the calcined material leading to a low surface functionality does not

provide stabilisation of the metal clusters within the channels. Therefore, only non-calcined (extracted) samples of the mesoporous silicas were used for further experiments.

Palladium loading in the mesoporous materials was varied in the range from 0.1 to 4.4 wt.%. It was confirmed by N_2 adsorption–desorption measurements that the metal-containing silicas retained their mesoporous structures, showing a high specific surface area and narrow pore size distribution (see Table 1 and Figs. 1–3). At the same time, the XRD investigations of the Pd/HMS composite materials revealed that the X-ray diffraction peak intensity decreased with increasing the metal loading (Fig. 4). Metal introduction seems to disturb the local symmetry in the channel packing and leads to a loss in the integrity of the worm-like HMS framework structure [55]. In contrast, the Pd/SBA-15 composites conserve the well-ordered 2D hexagonal array of the support (Fig. 5). A large SBA-15 framework wall thickness (Table 1) may be the reason for the increased stability [15].

The SSA and specific pore volume of the HMS and SBA-15 Pd-containing silicas only slightly decrease with metal loading. The average pore size of the materials was found to remain practically unchanged. This result suggests that the formation of Pd particles within the mesoporous silicas did not lead to the destruction or blocking of the mesoporous framework channels.

The 2.1%Pd/SBA-15-red., which was directly reduced after Pd deposition on the SBA-15-extr., demonstrated ~100% metal dispersion ($d_{Pd} \sim 1$ nm). A dispersion close to 100% was also observed for the calcined Pd/HMS-extr. samples with low Pd loading of 0.1–0.2 wt.% (Table 1). The increase of the metal content in the Pd/HMS-extr. and Pd/SBA-15-extr. samples from 0.25 to 4.4 wt.% left an average metal particle size practically unchanged: 1.4–1.9 and 3.5–3.6 nm, respectively. In all cases, the average Pd particle diameter did not exceed the mesopore diameter, suggesting that the Pd clusters were formed within the confined mesopore space, and their maximum size was controlled by the pore diameter. As a result, the nanoparticles were resistant against sintering during calcination.

The TEM images of the 4.4%Pd/HMS(18)-extr. and 2.1%Pd/SBA-15-extr. samples (Figs. 6–8) provide further information on the Pd nanoparticles within the mesoporous silica framework channels. As seen in Fig. 6a, the 4.4%Pd/HMS(18)-extr. material consists of spherical monolithic grains. The framework mesopores are wormhole-like throughout the grain. No apparent long-range order in the pore arrangement was detected. Pd clusters are well dispersed within the silica matrices. The corresponding selected area electron

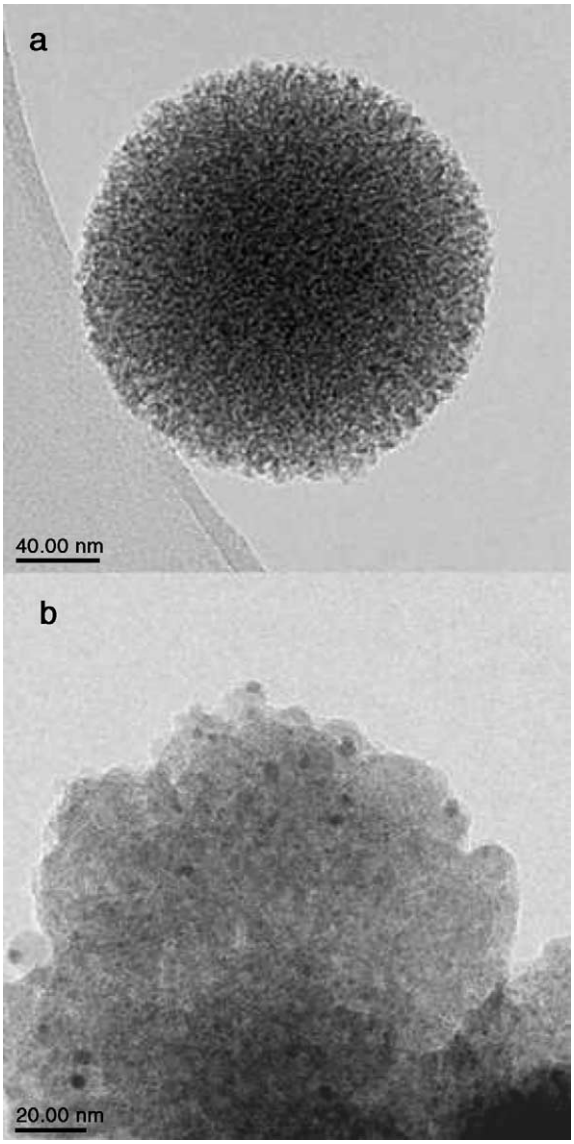

Fig. 6. Bright field TEM images of the 4.4%Pd/HMS(18)-extr.: (a) a spherical grain: the image was slightly under-focused to enhance visibility of the worm-like porous structure; (b) Pd nanoparticles within the mesoporous silica grain.

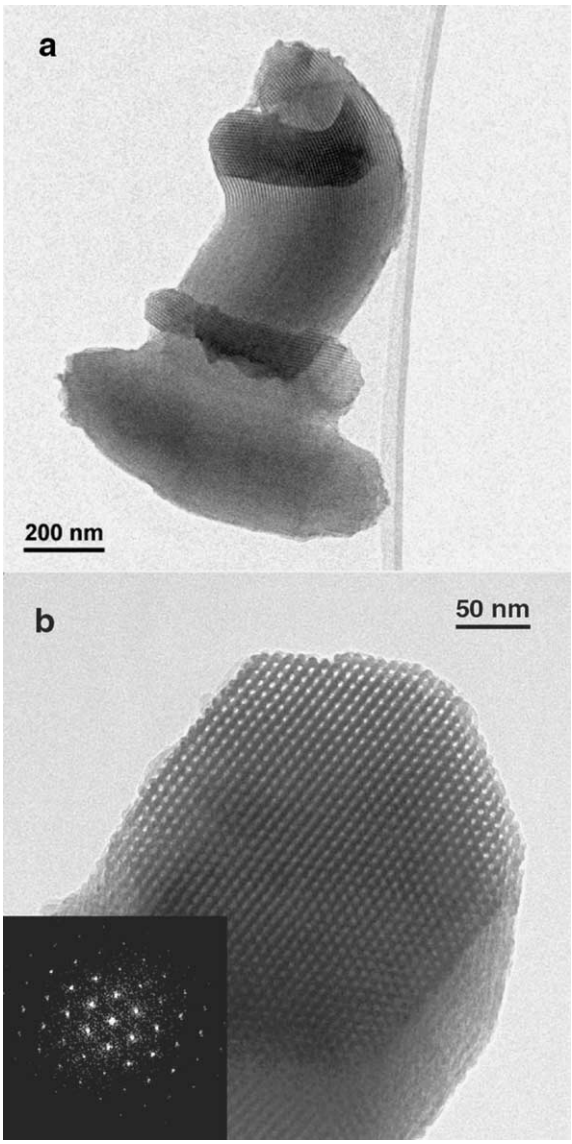

Fig. 7. Bright field TEM images of the 2.1%Pd/SBA-15-extr.: (a) several grains stuck together; (b) the prismatic array of pores with hexagonal symmetry.

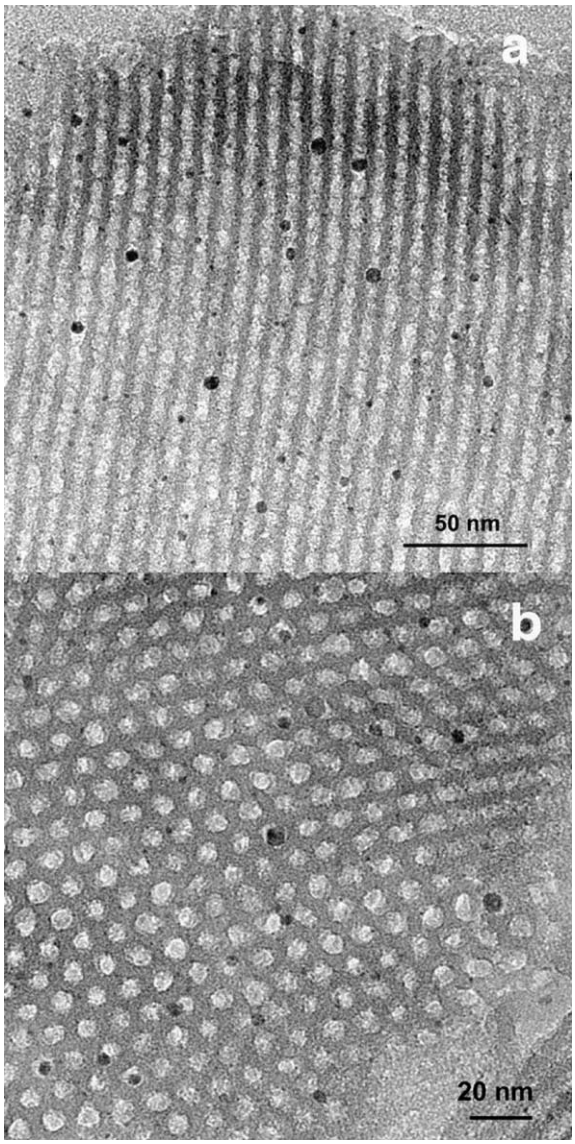

Fig. 8. Pd nanoparticles within the framework channels of the 2.1%Pd/SBA-15-extr. The bright field TEM images for the slices prepared by ultramicrotomy: (a) the electron beam was perpendicular, and (b) the electron beam was parallel to the main axis of the mesopores.

diffraction pattern revealed that the crystalline nature of the Pd particles was the same as that of bulk palladium. Most of Pd particles seen in Fig. 6b have a diameter ($d_{Pd} < 3.5$ nm), which does not exceed the average pore diameter ($D_{av} \sim 3.6$ nm). Because of the large thickness and the amorphous nature of the mesoporous support, the determination of the size and the location of the Pd nanoparticles was hindered. However, the obtained experimental data suggest that small Pd clusters were formed and stabilised in the mesoporous silica channels.

The TEM image of the 2.1%Pd/SBA-15-extr. (Fig. 7a) shows material grains with a regular array of

mesopores. Observation along a direction close to the pore axis (Fig. 7b) revealed a prismatic structure with a hexagonal cross-section of *p6mm* plane group symmetry [14]. The observed distance between the pore rows (8.6 ± 0.4 nm) and pore diameter ($D \sim 4.5$ nm) are in a reasonable agreement with the value from the XRD ($d_{100} \sim 9.2$ nm) and N_2 adsorption measurements ($D_{av} \sim 5.1$ nm). As clearly seen on the image of the 2.1%Pd/SBA-15-extr. sample prepared by ultramicrotomy (Fig. 8), Pd nanoparticles are well dispersed within the mesoporous silica and isolated from each other. Their size ($d_{Pd} = 2$–4 nm) does not exceed the mesopore diameter ($D \sim 4.5$ nm). Most of the nanocrystals are located within the mesoporous framework channels. Thus, the TEM investigation gives a consistent evidence of the strong anchoring of the Pd precursor on the SBA-15 mesopore walls and the confining effect of the silica mesoporous framework during the Pd clusters formation. However, it should be noted that a few of the metal particles were detected to be outside the mesopores. The biggest of them ($d_{Pd} = 6$–10 nm) were situated on the external silica grain surface near the mesopores entries resulting from the uncontrolled metal particle growth. Sometimes, small Pd nanocrystals were found within the walls (Fig. 8). It is probable that these Pd nanoparticles are located in the complementary pores, which are known to connect the primary mesopores of SBA-15 [58–60].

Low mechanical strength and collapsing of the structure at elevated temperature in the presence of water are the main drawbacks of mesoporous materials limiting their use as catalysts. In order to investigate the stability of the synthesised materials under real reaction conditions, the 2.1%Pd/SBA-15-extr. was tested in methane combustion (Fig. 9). Only CO_2 and H_2O were found as the reaction products. The CH_4 conversion of ~85% was achieved over the catalyst at 520 °C and GHSV $= 30\,m^3_{CH_4}/h/kg_{Pd}$. The catalytic activity was stable during the long-term operation (6 h). The measurements performed after the reaction revealed that the specific surface area of the material dropped from 730 to 690 m^2/g, and the average metal particle size only slightly increased from 3.5 to 4.0 nm. The SBA-15 support and Pd nanoparticles confined within the mesopores under the mentioned

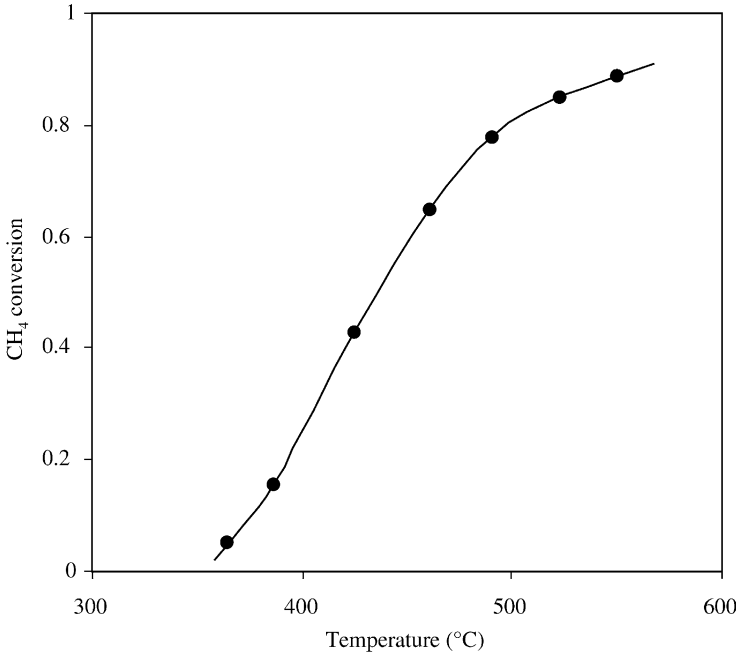

Fig. 9. Temperature dependence of methane conversion over the 2.1%Pd/SBA-15-extr. catalyst: GHSV $= 30\,m^3_{CH_4}/h/kg_{Pb}$; $C_{CH_4} = 1$ vol.%; $C_{O_2} = 10$ vol.%.

reaction conditions were seen to be quite resistant against structure collapsing and metal sintering.

4. Conclusions

1. Synthesis of Pd nanoparticles of 1–3.6 nm in mesoporous silicas was performed, using non-calcined HMS and SBA-15, prepared by solvent extraction of the templates. High concentration of silanol groups on the non-calcined mesopore surface provided its high ion-exchange capacity. At the same time, the solvent extraction allows the recovering of valuable templates. Pd was deposited via ion-exchange of surface silanol groups with $[Pd(NH_3)_4]^{2+}$ followed by air-calcination (550 °C, 4 h) and/or reduction by H_2 (300 °C, 1 h). The Pd loading was varied in the range from 0.1 to 4.4 wt.%.
2. The Pd/HMS and Pd/SBA-15 were characterised by a high SSA and narrow pore size distribution. Introduction of Pd nanoparticles into HMS seems to disturb the local symmetry in the channel packing, destroying the original structure of HMS silica. In contrast, the Pd/SBA-15 composites retained the well-order 2D hexagonal structure, probably due to the thicker mesopore walls.
3. The Pd particle size was shown to be controlled by the silica framework. The TEM investigations of the 2.1%Pd/SBA-15-extr. revealed that most of Pd nanoparticles were located inside the mesoporous channels. However, a small amount of metal nanocrystals was detected within the pore walls indicating the presence of the complementary pores, connecting the primary mesopores of SBA-15. The size of Pd particles formed within the confined space of the mesopores did not exceed the mesopore diameter even at relatively high metal loadings and after heating in air at 550 °C for 4 h.
4. The catalyst 2.1%Pd/SBA-15-extr. demonstrated stable activity and no metal agglomeration during methane combustion at 520 °C for 6 h.

Acknowledgements

The authors thank the Swiss Commission of Technology and Innovation (CTI, Bern) for the financial support in the framework of TOPNANO 21 program. The work of Mr. E. Casali for the N_2 adsorption–desorption measurements and Mrs. A. Udriot for the chemical analysis is highly appreciated.

References

[1] L.J. de Jongh, Physics and Chemistry of Metal Cluster Compounds, Kluwer Academics Publishers, Dordrecht, 1994.
[2] F. Piuz, J.P. Borel, Phys. Status Solidi A 14 (1972) 129.
[3] P. Buffat, J.-P. Borel, Phys. Rev. A 13 (1976) 2287.
[4] P.M. Ajayan, L.D. Marks, Phys. Rev. Lett. 60 (1988) 585.
[5] M. Haruta, Catal. Today 36 (1997) 153.
[6] N. Herron, D. Thorn, Adv. Mater. 10 (1998) 1173.
[7] P. Armand, M.-L. Saboungi, D.L. Price, L. Iton, C. Cramer, M. Grimsditch, Phys. Rev. Lett. 79 (1997) 2061.
[8] A. Fukuoka, N. Higashimoto, Y. Sakamoto, M. Sasaki, N. Sugimoto, S. Inagaki, Y. Fukushima, M. Ichikawa, Catal. Today 66 (2001) 23.
[9] H. Maeda, Y. Kinoshita, K.R. Reddy, K. Muto, S. Komai, N. Katada, M. Niwa, Appl. Catal. A: Gen. 163 (1997) 59.
[10] J.S. Beck, J.C. Vartuli, W.J. Roth, M.E. Leonowicz, C.T. Kresge, K.D. Schmitt, C.T. Chu, D.H. Olsen, E.W. Sheppard, S.B. McCullen, J.B. Higgins, J.L. Schlenker, J. Am. Chem. Soc. 114 (1992) 10835.
[11] C.T. Kresge, M.E. Leonowicz, W.J. Roth, J.C. Vartuli, J.S. Beck, Nature 359 (1992) 710.
[12] Q. Cai, W.-Y. Lin, F.-S. Xiao, W.-Q. Pang, X.-H. Chen, B.-S. Zou, Micropor. Mesopor. Mater. 32 (1999) 1.
[13] Q. Huo, D.I. Margolese, U. Ciesla, D.G. Demuth, P. Feng, T.E. Gier, P. Sieger, A. Firouzi, B.F. Chemelka, F. Schüth, G.D. Stucky, Chem. Mater. 6 (1994) 1176.
[14] D. Zhao, J. Feng, Q. Huo, N. Melosh, G.H. Fredrickson, B.F. Chmelka, G.D. Stucky, Science 279 (1998) 548.
[15] D. Zhao, Q. Huo, J. Feng, B.F. Chmelka, G.D. Stucky, J. Am. Chem. Soc. 120 (1998) 6024.
[16] P.T. Tanev, T.J. Pinnavaia, Science 267 (1995) 865.
[17] S.A. Bagshaw, E. Prouzet, T.J. Pinnavaia, Science 269 (1995) 1242.
[18] D. Trong On, D. Desplantier-Giscard, C. Danumah, S. Kaliaguine, Appl. Catal. A: Gen. 222 (2001) 299.
[19] R.C. Hayward, P. Alberius-Henning, B.F. Chmelka, G.D. Stucky, Micropor. Mesopor. Mater. 44/45 (2001) 619.
[20] K. Moller, T. Bein, Chem. Mater. 10 (1998) 2950.
[21] W. Chen, W.P. Cai, Y. Lei, L.D. Zhang, Mater. Lett. 50 (2001) 53.
[22] E. Paetzold, G. Oehme, H. Fuhrmann, M. Richter, R. Eckelt, M.M. Pohl, H. Kosslick, Micropor. Mesopor. Mater. 44/45 (2001) 517.
[23] K.B. Lee, S.M. Lee, J. Cheon, Adv. Mater. 13 (2001) 517.
[24] Y.C. Wu, L. Zhang, G.H. Li, C.H. Liang, X.M. Huang, Y. Zhang, G.M. Song, J.H. Jia, Z.X. Chen, Mater. Res. Bull. 36 (2001) 253.
[25] P. Magnoux, N. Lavaud, M. Guisnet, Top. Catal. 13 (2000) 291.

[26] B.M. Choudary, M.L. Kantam, N.M. Reddy, K.K. Rao, Y. Haritha, V. Bhaskar, F. Figueras, A. Tuel, Appl. Catal. A: Gen. 181 (1999) 139.
[27] M. Shirai, N. Suzuki, Y. Nishiyama, K. Torii, M. Arai, Appl. Catal. A: Gen. 177 (1999) 219.
[28] C.P. Mehnert, D.W. Weaver, J.Y. Ying, J. Am. Chem. Soc. 120 (1998) 12289.
[29] C.A. Koh, R. Nooney, S. Tahir, Catal. Lett. 47 (1997) 199.
[30] M. Ohtaki, K. Inata, K. Eguchi, Chem. Mater. 10 (1998) 2582.
[31] C.P. Mehnert, J.Y. Ying, Chem. Commun. 20 (1998) 2215.
[32] L. Bronstein, E. Krämer, B. Berton, C. Burger, S. Förster, M. Antonietti, Chem. Mater. 11 (1999) 1402.
[33] L.M. Bronstein, S. Polarz, B. Smarsly, M. Antonieti, Adv. Mater. 13 (2001) 1333.
[34] U. Junges, W. Jacobs, I. Voigt-Martin, B. Krutzsch, F. Schüth, J. Chem. Soc., Chem. Commun. (1995) 2283.
[35] R. Long, R.T. Yang, Catal. Lett. 52 (1998) 91.
[36] Y.-J. Han, J.M. Kim, G.D. Stucky, Chem. Mater. 12 (2000) 2068.
[37] M.A. Aramendia, V. Borau, C. Jimenez, J.M. Marinas, F.J. Romero, F.J. Urbano, Acta Mater. 49 (2001) 1957.
[38] N. Yao, C. Pinckey, S. Lim, C. Pak, G.L. Haller, Micropor. Mesopor. Mater. 44/45 (2001) 377.
[39] Q.-H. Xia, K. Hidajat, S. Kawi, Catal. Today 68 (2001) 255.
[40] M. Sasaki, M. Osada, N. Higashimoto, T. Yamamoto, A. Fukuoka, M. Ichikawa, J. Mol. Catal. A Chem. 141 (1999) 223.
[41] G.S. Attard, S.A.A. Leclerc, S. Maniguet, A.E. Russell, I. Nandhakumar, P.N. Bartlett, Chem. Mater. 13 (2001) 1444.
[42] S. Hermans, R. Raja, J.M. Thomas, B.F.G. Johnson, G. Sankar, D. Gleeson, Angew. Chem. Int. Edit. 40 (2001) 1211.
[43] M. Florea, M. Sevinci, L.G. Pârvulescu, S. Kaliaguine, Micropor. Mesopor. Mater. 44/45 (2001) 483.
[44] F. Schweyer, P. Braunstein, C. Estournes, J. Guille, H. Kessler, J.L. Paillaud, J. Rose, Chem. Commun. 14 (2000) 1271.
[45] M. Hartmann, C. Bischof, Z. Luan, L. Kevan, Micropor. Mesopor. Mater. 44/45 (2001) 385.
[46] D. Ozkaya, W.Z. Zhou, J.M. Thomas, P. Midgley, V.J. Keast, S. Hermans, Catal. Lett. 60 (1999) 113.
[47] H.B. Jervis, M.E. Raimondi, R. Raja, T. Maschmeyer, J.M. Seddon, D.W. Bruce, Chem. Commun. (1999) 2031.
[48] H.Z. Shi, L.D. Zhang, W.P. Cai, Mater. Res. Bull. 35 (2000) 1689.
[49] W. Chen, W.P. Cai, G.Z. Wang, L. Zhang, Appl. Surf. Sci. 174 (2001) 51.
[50] Y. Guari, C. Thieuleux, A. Mehdi, C. Reyé, J.P. Corriu, S. Gomez-Gallardo, K. Rhilippot, B. Chaudret, R. Dutartre, Chem. Commun. 15 (2001) 1374.
[51] M. Okumura, S. Tsubota, M. Iwamoto, M. Haruta, Chem. Lett. 4 (1998) 315.
[52] M.H. Huang, A. Choudrey, P.D. Yang, Chem. Commun. 12 (2000) 1063.
[53] J. Michalik, D. Brown, J.-S. Yu, M. Danilczuk, J.Y. Kim, L. Kevan, Phys. Chem. Chem. Phys. 3 (2001) 1705.
[54] L. Mercier, T.J. Pinnavaia, Environ. Sci. Technol. 32 (1998) 2749.
[55] T.R. Pauly, T.J. Pinnavaia, Chem. Mater. 13 (2001) 987.
[56] L. Kiwi-Minsker, I. Yuranov, E. Slavinskaya, V. Zaikovskii, A. Renken, Catal. Today 59 (2000) 61.
[57] P.T. Tanev, J. Chem. Mater. 8 (1996) 2066.
[58] M. Kruk, M. Jaroniec, Chem. Mater. 12 (2000) 1961.
[59] M. Imperor-Clerc, P. Davidson, A. Davidson, J. Am. Chem. Soc. 112 (2000) 11925.
[60] R. Ryoo, C.H. Ko, M. Kruk, M. Jaroniec, J. Phys. Chem. B 104 (2000) 11465.